Single-Molecule Electrochemical Transistor Utilizing a Nickel-Pyridyl Spinterface

Richard J. Brooke,[†] Chengjun Jin,[‡] Doug S. Szumski,[†] Richard J. Nichols,[¶]

Bing-Wei Mao,[§] Kristian S. Thygesen,[∗,‡] and Walther Schwarzacher[∗,†]

H. H. Wills Physics Laboratory, University of Bristol, Tyndall Avenue, Bristol BS8 1TL,
United Kingdom, Center for Atomic-Scale Materials Design (CAMD) and Center for
Nanostructured Graphene (CNG), Department of Physics, Technical University of
Denmark, DK2800 Kongens Lyngby, Denmark, Department of Chemistry, University of
Liverpool, Liverpool, L69 7ZD, United Kingdom, and State Key Laboratory of Physical
Chemistry of Solid Surfaces, Chemistry Department, College of Chemistry and Chemical
Engineering, Xiamen University, Xiamen 361005, China

E-mail: thygesen@fysik.dtu.dk; w.schwarzacher@bristol.ac.uk

───────────────

[∗]To whom correspondence should be addressed
[†]H. H. Wills Physics Laboratory, University of Bristol, Tyndall Avenue, Bristol BS8 1TL, United Kingdom
[‡]Center for Atomic-Scale Materials Design (CAMD) and Center for Nanostructured Graphene (CNG), Department of Physics, Technical University of Denmark, DK2800 Kongens Lyngby, Denmark
[¶]Department of Chemistry, University of Liverpool, Liverpool, L69 7ZD, United Kingdom
[§]State Key Laboratory of Physical Chemistry of Solid Surfaces, Chemistry Department, College of Chemistry and Chemical Engineering, Xiamen University, Xiamen 361005, China

Abstract

Using a scanning tunnelling microscope break-junction technique, we produce 4,4'-bipyridine (44BP) single-molecule junctions with Ni and Au contacts. Electrochemical control is used to prevent Ni oxidation, and to modulate the conductance of the devices via non-redox gating - the first time this has been shown using non-Au contacts. Remarkably the conductance and gain of the resulting Ni-44BP-Ni electrochemical transistors is significantly higher than analogous Au-based devices. Ab-initio calculations reveal that this behaviour arises because charge transport is mediated by spin-polarized Ni d-electrons, which hybridize strongly with molecular orbitals to form a 'spinterface'. Our results highlight the important role of the contact material for single-molecule devices, and show that it can be varied to provide control of charge and spin transport.

Keywords

Single-molecule, Break-junction, Electrochemical gating, Spintronics, Density functional theory, Metal-molecule interface

Main Text

Single-molecule transistor behaviour can be achieved using a gate electrode to control the energy levels of a molecule bridging two metallic electrodes.[1] This gate can be provided electrochemically using the double layer potential existing at the metal-electrolyte interface (Fig. 1**a**). An electrochemical gate avoids the complex fabrication of solid-state three-terminal molecular devices, can operate in room temperature liquid environments, and can produce high gate efficiencies thanks to the large electric fields which are achievable. There has been significant interest in redox active molecules such as viologens as candidates for electrochemical transistors,[2–4] however the gating of non-redox molecules has only recently been demonstrated using Au electrodes by Li et al.[5] with 4,4'-bipyridine (44BP) molecules,

and subsequently by Capozzi et al.[6] Non-redox gating relies directly on the modulation of the electronic energy levels of the molecule and the contacts, and closely resembles the operation of the traditional field-effect transistor.

The metal-molecule contact plays a critical role in molecular electronics.[7] Au-pyridyl contacts, such as the Au-44BP bond, have been shown to provide reproducible junctions for which two conductance values can be distinguished due to different binding geometries.[8–10] However, despite significant progress investigating different chemical linker groups[9,11–18] there have been few previous attempts to broaden the range of metal electrodes studied. The use of other metals promises a better understanding of the metal-molecule interface and new effects for molecular devices. For example, ferromagnetic contacts such as Ni are anticipated to deliver single-molecule spintronic effects.[19,20] Spin-dependent orbital hybridization at the metal-molecule interface was previously demonstrated at low temperature[21] and more recently at room temperature by Lee et al.[22] who showed that it strongly affects thermopower of Ni-benzenedithiol-Ni single-molecule junctions.

Using a scanning tunnelling microscope (STM) break junction technique[23] we fabricate 44BP single-molecule electrochemical transistors with Ni and Au contacts, utilizing electrochemical control to prevent oxidation of the Ni contacts and to provide non-redox electrochemical gating of the devices. The Ni devices exhibit significant advantages compared to Au-based ones, including larger conductance and more stable chemical binding due to the influence of the Ni d-electrons. They also exhibit stronger electrochemical transistor behaviour. Density functional theory (DFT) based calculations show that the microscopic origin of the gating is fundamentally different for Ni and Au based junctions due to the strong hybridisation of the Ni d-electrons with the frontier molecular orbitals and the ferromagnetic nature of the Ni contacts, which is consistent with the findings of Lee et al.[22]

Electrochemical control was provided by a four-electrode electrochemical cell which is shown schematically in Fig. 1a. The potentials of the STM tip and substrate were controlled relative to that of the electrolyte, which consisted of a pH 3 0.05 M Na_2SO_4 aqueous
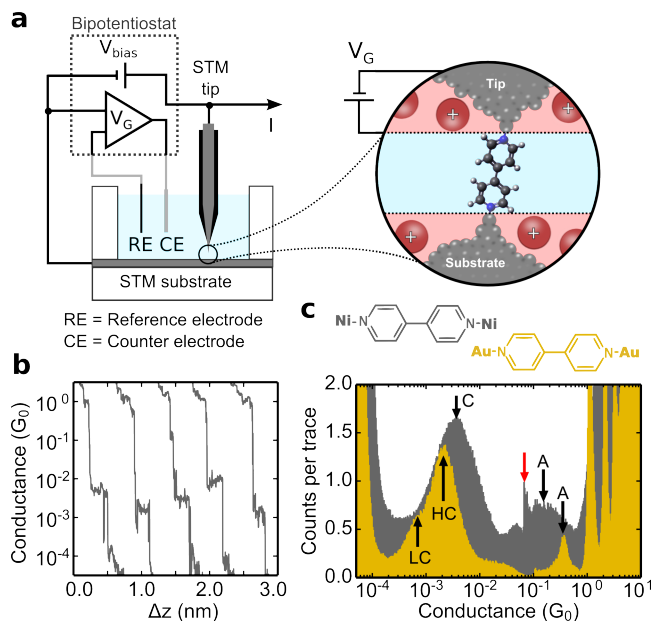
Figure 1: (a) Schematic diagram of the 4-electrode cell and cartoon of the electrochemical double layer over which the gate voltage (V_G) is applied. (b) Example conductance-distance traces obtained for Ni-44BP-Ni single-molecule junctions with a substrate potential of -0.9 V. Δz is the relative displacement of the tip which is offset laterally in each scan for clarity. (c) Logarithmically binned conductance histograms for Ni (grey) and Au (yellow) junctions generated from 1441 and 2200 scans, respectively, obtained at -0.9 V without data selection. The spike-like feature (labelled with a red arrow) is an artefact of the dual-channel pre-amplifier used for the measurements (see Supporting Information).

solution. A Pt wire was used as a counter electrode, and a polypyrrole quasi-reference electrode (PPy) was used.[24] This was found to have an open circuit potential of +0.31 V with respect to a saturated calomel reference electrode. Au substrates were obtained commercially and were prepared by cleaning in piranha solution, a 3:1 mixture of H_2SO_4 and H_2O_2 (WARNING: piranha solution is dangerous and should be prepared and used with caution). Ni substrates were prepared by the electrodeposition of a $\sim$ 100 nm Ni coating onto clean Au substrates. Ni and Au STM tips were produced by electrochemical etching[25,26] and were coated with wax to minimise unwanted electrochemical currents. Ni oxide was removed by in-situ electrochemical reduction.[27] To ensure the magnetic configuration of the Ni electrodes remained constant during the conductance measurements, a custom built electromagnet was used to provide a 2 kOe magnetic field parallel to the substrate surface.

Conductance-distance traces were obtained by measuring current through the STM tip whilst repeatedly withdrawing it from contact with the substrate surface. During each conductance-distance measurement the tip was first brought to a set-point current of 400 μA before the feedback was disabled and the tip retracted by 6 nm at a rate of 20 nm s^{-1}. Fig. 1**b** shows selected traces obtained using Ni electrodes under electrochemical control in a solution containing 44BP molecules. Plateaus observed in these traces which have $G \geq G_0$ (where G_0 is the conductance quantum $2e^2/h$) are attributed to spontaneous atomic restructuring of the metal contacts as they are stretched. Before the metal contact is broken, traces generally exhibit a plateau close to G_0 indicating the formation of single-atom contacts. After the initial separation of the newly formed contacts, a single-molecule can bridge them. In this case a plateau is observed in the conductance-distance trace, otherwise we observe an exponential decay of the tunnelling current (see Supporting Information). In each experiment, conductance histograms were generated from several thousand conductance traces. To avoid possible bias, no selection or filtering was applied to the data. A constant tip-substrate voltage of 0.1 V was maintained throughout the experiments, whilst the potential of the substrate with respect to the surrounding electrolyte was varied between measurements in order to modulate the gate voltage.

Fig. 1**c** compares typical logarithmically binned conductance histograms obtained for Ni and Au junctions in the presence of 44BP under electrochemical control. Plateaus in the conductance traces give rise to clear features in the histograms. Pronounced peaks are observed in the Au histograms for $G \geq G_0$ due to the existence of preferred atomic configurations for the contacts. Even though Ni conductance traces exhibit clear plateaus for $G \geq G_0$ variation between individual traces leads to only a single broad peak in the histogram similar to previous reports of Ni atomic contacts[28] (see Supporting Information). Additional peaks (labelled A) observed between 0.1 G_0 and 1 G_0 are attributed to the effects of hydrogen adsorption on the atomic contacts[5,29] (see Supporting Information). Molecular features appear in the histograms with $G \ll G_0$ only when 44BP molecules are present. High
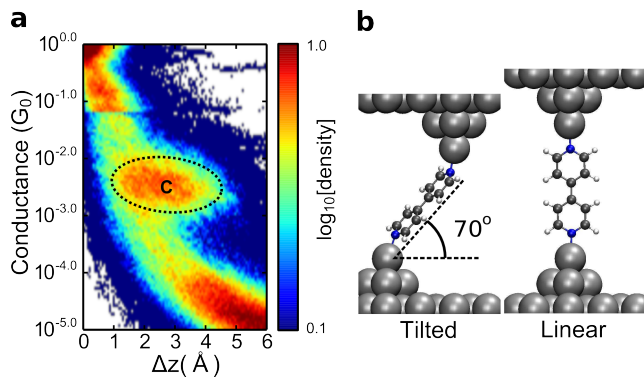
5

Figure 2: (a) 2d conductance histogram obtained for electrochemically controlled Ni-44BP-Ni molecular junctions with a substrate potential of -0.9 V (with respect to the PPy electrode). The individual conductance traces were offset laterally to synchronize the start of each scan with the end of the final atomic metal plateau in the range $0.8 - 2$ G_0. As such some data selection was carried out since only scans with a plateau in this range were included. This selection was done using an automated algorithm. The histogram contains 1817 out of 2520 scans. (b) The 44BP molecule in the tilted junction geometry and linear geometry.

conductance and low conductance features (labelled HC and LC), which are typical of the Au-pyridyl contact[8–10] are observed for Au, whereas only a single broad peak (labelled C) which has larger conductance than the Au features is observed for Ni contacts. Compared with Au, Ni junctions show considerable trace-to-trace conductance variation, leading to a broader peak in the histogram, which is similar to recently reported Ag molecular junctions.[30]

The differences between Ni and Au junctions are also reflected in 2-dimensional (2d) histograms. In agreement with previous results[8] the Au histogram (see Supporting Information) exhibits two clearly distinguishable areas with a high number of counts due to the separate HC and LC configurations, whereas in Fig. 2a only a single feature is seen for Ni junctions. In the initial stage of the junction evolution, the molecule is most likely tilted with respect to the junction axis, since 44BP molecules are larger than the average initial electrode separation of 2.5 Å or 4.0 Å for Ni or Au contacts, respectively (see Supporting Information), so that the molecules are swept through a range of contact angles as the tip is retracted. In the case of Au-44BP-Au junctions, our DFT-based calculations (see later) predict a higher conductance when the molecule is tilted compared to when it is linear (see Fig. 2b) with binding energies for the two configurations of 1.71 eV and 1.91 eV respec-
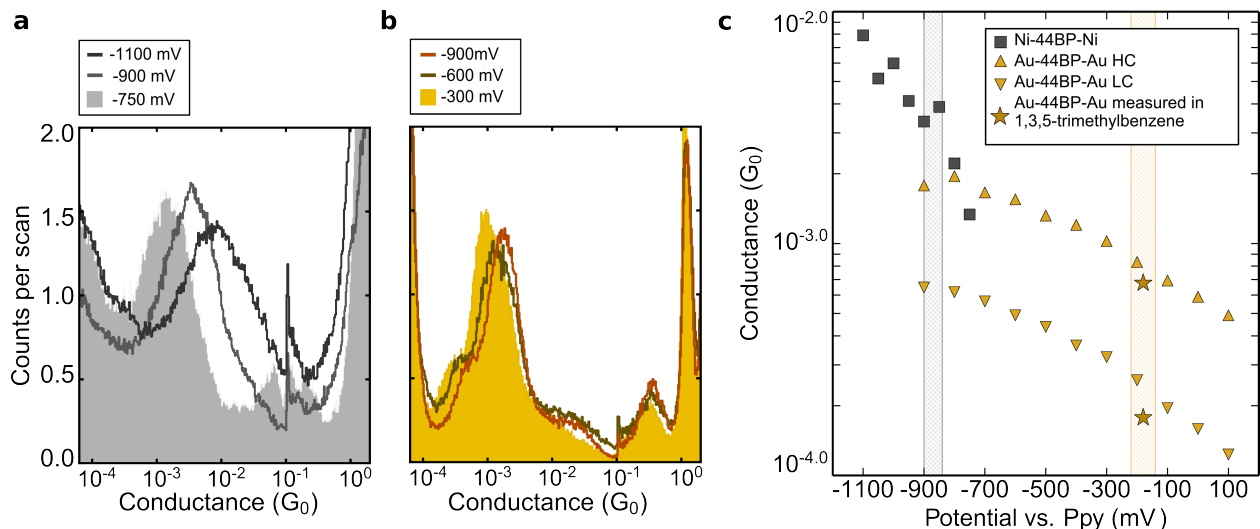
6

Figure 3: Conductance histograms obtained for Ni-44BP-Ni (a) and Au-44BP-Au (b) single-molecule junctions with various different potentials applied to the substrate. (c) The mean conductance values measured for Ni-44BP-Ni and Au-44BP-Au junctions under electrochemical control are plotted as a function of substrate potential. The conductance values measured for Au-44BP-Au junctions in 1,3,5-trimethylbenzene solvent are plotted at the potential of zero charge (PZC) of Au electrodes in a non-specifically adsorbing $HClO_4$ electrolyte, which is -0.18 V vs. the PPy scale.[31] The PZCs for Ni (-0.87 V vs. PPy[31]) and Au electrodes in $HClO_4$ are indicated by the grey and gold shaded regions respectively. (PPy = +0.31 V vs. SCE)

tively, in good agreement with previous results.[8] Our calculations for Ni junctions show that 44BP binds more strongly to Ni than to Au by almost 1 eV, yielding binding energies for the tilted and linear configurations of 2.64 eV and 2.54 eV, respectively. According to the DFT-based transport calculations, the tilted and linear configurations are also found to have similar conductance (see Supporting Information), in contrast to the case of Au electrodes. This suggests that both configurations are probed in the Ni break junction experiments, but are indistinguishable from each other because the conductance is insensitive to the contact angle, which is consistent with the single feature in the histograms.

Fig. 3a and 3b show that the conductance of Ni-44BP-Ni and Au-44BP-Au junctions vary as a function of the gate voltage applied to the substrate. The molecular peaks are clearly shifted to higher conductance values as the potential is made more negative. At potentials more positive than -0.7 V no molecular junctions were observed for Ni contacts,

which is likely due to the onset of Ni oxidation. The mean conductance was extracted from each histogram by fitting a log-normal distribution to the molecular conductance peak. These values are plotted in Fig. 3**c**. For both Au and Ni contacts the conductance increases exponentially as the potential is made more negative. The conductance of Ni junctions is larger and the gate voltage dependence is stronger. In the case of Au the conductance reaches a plateau at negative potentials, which was not observed in previous studies covering a less extensive potential range.[5,6] The gating effect can be explained by a change in the Fermi level of the electrodes (ϵ_F) relative to that of the molecule due to the potential applied between the electrodes and the solution in which the molecule is situated. As the potential is made more negative, ϵ_F is raised and the energy barrier for electron tunnelling between ϵ_F and the lowest unoccupied molecular orbital (LUMO) decreases.[5] The conductances of Au-44BP-Au junctions measured in non-polar 1,3,5 trimethylbenzene solvent (where no electrochemical gating is possible) are also plotted in Fig. 3**c** at the potential of zero charge of Au electrodes in non-specifically adsorbing $HClO_4$ electrolyte (PZC), where no gating effect is expected[5] and where there is good agreement with the measurements performed in the electrochemical environment. Measurements were also performed using 1,2-bis(4-pyridyl)ethylene which exhibits similar trends to 44BP based molecular junctions (See Supporting Information).

Our results are corroborated by DFT-based calculations of the conductance which were performed using the non-equilibrium Green's function method in the GPAW code.[32] The DFT energies were corrected to account for self-interaction errors and missing image charge screening.[16] The linear conductance was calculated from the Laudauer formula,[33] and the effect of the electrochemical gate was simulated in a non self-consistent way by shifting the energy levels of the molecular orbitals by a constant V_G. We also performed extensive many-body GW calculations[34] for the non-gated linear and tilted Au junctions. The GW calculations are in good agreement with the DFT-based results which further validates the use of the DFT-based transport scheme (see Supporting Information). Further details of the theoretical methods are described in the Supporting Information. Fig. 4 shows the
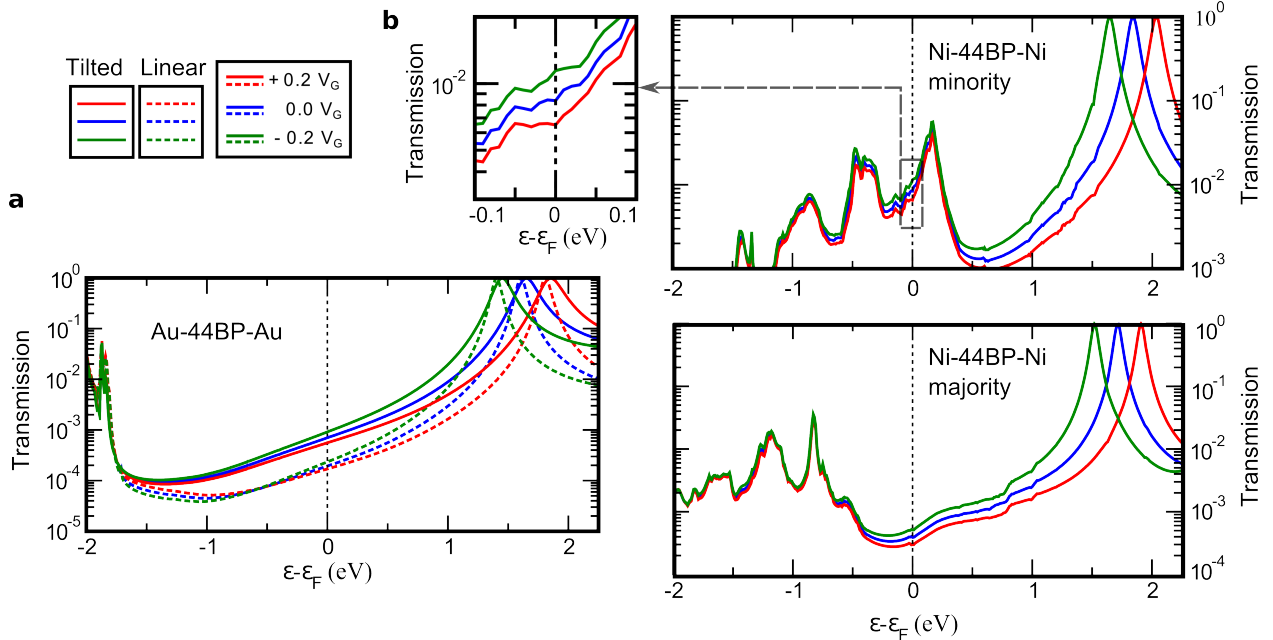
Figure 4: Transmission functions calculated at different gate voltages for (a) Au-44BP-Au junctions in the tilted configuration (solid lines), and the linear configuration (dashed lines), and (b) spin-polarized Ni-44BP-Ni junctions in the tilted configuration. The upper panel shows the Ni minority spin channel, and the lower panel shows the majority channel. The inset shows a zoomed-in area of the transmission curves around the Fermi energy for the minority channel with different gate voltages. For clarity the linear configuration is not shown but the transmission at ϵ_F is very similar to that of the tilted configuration (See Supporting Information).

relevant electron transmission curves calculated using DFT-based methods for Au-44BP-Au and Ni-44BP-Ni junctions at various different values of gate voltage. These transmission curves show how the probability of an electron to be transmitted through the junction varies as a function of electron energy. Conductances calculated from such transmission curves are compared to the measured values in Fig. 5. The potential difference between the Ni or Au electrodes and the reference electrode is equal to V_G plus an offset that depends on the choice of reference electrode. We assume that $V_G = 0$ corresponds to the PZC of each electrode (see previously and SI). Using this assumption in Fig. 5 provides good agreement between the calculations and the measurements performed in the electrochemical environment.

For the Au-44BP-Au transmission curves (Fig. 4a), the tail of the LUMO resonance dominates the transmission at ϵ_F. In agreement with previous work the stronger electronic
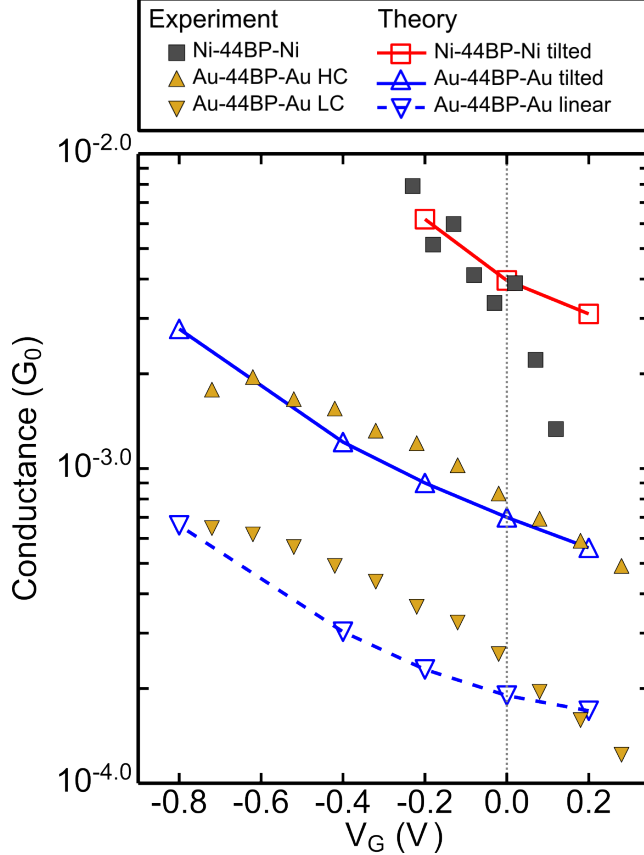
Figure 5: Comparison of the conductance calculated for Au-44BP-Au junctions and spin-polarized Ni-44BP-Ni junctions in the tilted configuration with experimentally measured values. The experimental data has been plotted so that measurements at the PZC of Ni (-0.87 V vs. PPy[31]) and Au (-0.18 V vs. PPy[31]) electrodes are located at $V_G = 0$.

coupling of the tilted configuration broadens the LUMO resonance, leading to higher transmission compared with the linear configuration at the same gate voltage.[10] As V_G is increased, ϵ_F is shifted closer to the LUMO resonance, and the transmission increases. In Fig. 5, the DFT calculations predict that the conductance of Au-44BP-Au junctions continues to rise at negative potentials, whereas experimentally the conductance reaches a plateau at around $V_G = -0.6$ V. A possible explanation is that the LUMO becomes pinned to ϵ_F at negative potentials due to charge transfer to the molecule from the electrodes leading to increased Coulomb repulsion. This pinning may prevent further gating of the Au devices and limit their potential as single-molecule transistors. The effect of this pinning is not captured in our DFT-based calculations because the gating effect is simulated by shifting

the molecule levels rigidly, rather than by a self-consistent approach incorporating charge transfer between metal and molecule. Another explanation of this plateau (limitation of the gate voltage due to saturation of the charge in the electrochemical double layer) was ruled out by performing measurements in various different solutions (see Supporting Information).

Due to the ferromagnetic nature of the Ni electrodes, the spin degeneracy of the electron transport is lifted. Therefore the transmission curves calculated for Ni junctions (Fig. 4**b**) are separated into contributions from the minority and majority spin channels. Non spin-polarized DFT-based calculations were also carried out but these did not reproduce the experimentally observed conductance. Unlike spin-polarized calculations, the non spin-polarised calculations predict a large increase in the conductance of a Ni-44BP-Ni junction going from the tilted to the linear geometry (see Supporting Information) which is not observed experimentally (see Fig. 2). This shows the importance of including spintronic effects when simulating single-molecule junctions with ferromagnetic contacts.

In Fig. 4**b** the transmission curves calculated for Ni-44BP-Ni junctions exhibit additional peaks close to the LUMO. These are due to the strong hybridization of the Ni d-band with the LUMO of the molecule (see Supporting Information). For the minority spin channel, ϵ_F lies on this peak which leads to a high transmission at ϵ_F and the experimentally observed increase in conductance between Ni-44BP-Ni and Au-44BP-Au junctions. The spin-split hybridization of the Ni d-band with the LUMO of the molecule is similar to that recently reported for Ni-benzenedithiol-Ni single-molecule junctions.[22] Note that for the majority channel the peak due to the hybridization is much lower in energy and correspondingly contributes much less to the total transmission at ϵ_F. This is extremely important, because it implies that the current through the Ni-44BP-Ni junction is highly spin-polarized, in apparent contrast to Ni-benzenedithiol-Ni.[22]

As the gate voltage applied to the Ni-44BP-Ni junctions is increased, ϵ_F is shifted closer to the LUMO and the hybridization of the LUMO with the Ni d-band increases. As a result the peak due to hybridization for the minority channel is enhanced and the conductance

goes up. This gating mechanism is qualitatively different to that active in the case of Au contacts.

In summary, we have established that single-molecule junctions with oxide-free Ni contacts can be fabricated under electrochemical control. Our method could easily be extended to other base metals which are of interest as contacts for single-molecule devices. The Ni-44BP-Ni junctions show promise as single-molecule transistors as they exhibit larger conductance and stronger gating than Au devices. Furthermore, DFT calculations strongly suggest that the current across the junction is highly spin-polarized due to spin-dependent hybridization of the Ni d-band with the LUMO of 44BP. This indicates that Ni-44BP-Ni junctions are good candidates for single-molecule spintronic applications.

Author Information

Corresponding Author

*E-mail: w.schwarzacher@bristol.ac.uk

Notes

The authors declare no competing financial interest.

Acknowledgement

Supporting Information Available

Additional information on theoretical and experimental methods, and supporting results and figures.

This material is available free of charge via the Internet at `http://pubs.acs.org/`.

References

(1) Song, H.; Kim, Y.; Jang, Y. H.; Jeong, H.; Reed, M. A.; Lee, T. *Nature* **2009**, *462*, 1039–43.

(2) Kay, N. J.; Higgins, S. J.; Jeppesen, J. O.; Leary, E.; Lycoops, J.; Ulstrup, J.; Nichols, R. J. *J. Am. Chem. Soc.* **2012**, *134*, 16817–26.

(3) Xu, B.; Xiao, X.; Yang, X.; Zang, L.; Tao, N. *J. Am. Chem. Soc.* **2005**, *127*, 2386–7.

(4) Haiss, W.; van Zalinge, H.; Higgins, S. J.; Bethell, D.; Höbenreich, H.; Schiffrin, D. J.; Nichols, R. J. *J. Am. Chem. Soc.* **2003**, *125*, 15294–5.

(5) Li, C.; Mishchenko, A.; Wandlowski, T. *Top. Curr. Chem.* **2012**, *313*, 121–88.

(6) Capozzi, B.; Chen, Q.; Darancet, P.; Kotiuga, M.; Buzzeo, M.; Neaton, J. B.; Nuckolls, C.; Venkataraman, L. *Nano Lett.* **2014**, *14*, 1400–4.

(7) Lörtscher, E. *Nat. Nanotechnol.* **2013**, *8*, 381–4.

(8) Quek, S. Y.; Kamenetska, M.; Steigerwald, M. L.; Choi, H. J.; Louie, S. G.; Hybertsen, M. S.; Neaton, J. B.; Venkataraman, L. *Nat. Nanotechnol.* **2009**, *4*, 230–4.

(9) Kamenetska, M.; Quek, S. Y.; Whalley, a. C.; Steigerwald, M. L.; Choi, H. J.; Louie, S. G.; Nuckolls, C.; Hybertsen, M. S.; Neaton, J. B.; Venkataraman, L. *J. Am. Chem. Soc.* **2010**, *132*, 6817–21.

(10) Kim, T.; Darancet, P.; Widawsky, J. R.; Kotiuga, M.; Quek, S. Y.; Neaton, J. B.; Venkataraman, L. *Nano Lett.* **2014**, *14*, 794–8.

(11) Marqués-González, S.; Yufit, D. S.; Howard, J. A. K.; Martín, S.; Osorio, H. M.; García-Suárez, V. M.; Nichols, R. J.; Higgins, S. J.; Cea, P.; Low, P. J. *Dalton Trans.* **2013**, *42*, 338–41.

(12) Hong, W.; Manrique, D. Z.; Moreno-García, P.; Gulcur, M.; Mishchenko, A.; Lambert, C. J.; Bryce, M. R.; Wandlowski, T. *J. Am. Chem. Soc.* **2012**, *134*, 2292–304.

(13) Parameswaran, R.; Widawsky, J. R.; Vazquez, H.; Park, Y. S.; Boardman, B. M.; Nuckolls, C.; Steigerwald, M. L.; Hybertsen, M. S.; Venkataraman, L. *J. Phys. Chem. Lett.* **2010**, *1*, 2114–2119.

(14) Arroyo, C. R.; Leary, E.; Castellanos-Gómez, A.; Rubio-Bollinger, G.; González, M. T.; Agraït, N. *J. Am. Chem. Soc.* **2011**, *133*, 14313–9.

(15) Ie, Y.; Hirose, T.; Nakamura, H.; Kiguchi, M.; Takagi, N.; Kawai, M.; Aso, Y. *J. Am. Chem. Soc.* **2011**, *133*, 3014–22.

(16) Mowbray, D. J.; Jones, G.; Thygesen, K. S. *J. Chem. Phys.* **2008**, *128*, 111103.

(17) Park, Y. S.; Whalley, A. C.; Kamenetska, M.; Steigerwald, M. L.; Hybertsen, M. S.; Nuckolls, C.; Venkataraman, L. *J. Am. Chem. Soc.* **2007**, *129*, 15768–9.

(18) Quek, S. Y.; Venkataraman, L.; Choi, H. J.; Louie, S. G.; Hybertsen, M. S.; Neaton, J. B. *Nano Lett.* **2007**, *7*, 3477–82.

(19) Sanvito, S. *Nat. Phys.* **2010**, *6*, 562–564.

(20) Rocha, A. R.; García-Suárez, V. M.; Bailey, S. W.; Lambert, C. J.; Ferrer, J.; Sanvito, S. *Nat. Mater.* **2005**, *4*, 335–9.

(21) Kawahara, S. L.; Lagoute, J.; Repain, V.; Chacon, C.; Girard, Y.; Rousset, S.; Smogunov, A.; Barreteau, C. *Nano Lett.* **2012**, *12*, 4558–63.

(22) Lee, S. K.; Ohto, T.; Yamada, R.; Tada, H. *Nano Lett.* **2014**, *14*, 5276–5280.

(23) Xu, B.; Tao, N. J. *Science* **2003**, *301*, 1221–3.

(24) Ghilane, J.; Hapiot, P.; Bard, A. J. *Anal. Chem.* **2006**, *78*, 6868–72.

(25) Cavallini, M.; Biscarini, F. *Rev. Sci. Instrum.* **2000**, *71*, 4457.

(26) Lopes, M.; Toury, T.; de La Chapelle, M. L.; Bonaccorso, F.; Gucciardi, P. G. *The Rev. Sci. Instrum.* **2013**, *84*, 073702.

(27) Suzuki, T.; Yamada, T.; Itaya, K. *J. Phys. Chem.* **1996**, *100*, 8954–8961.

(28) Kiguchi, M.; Konishi, T.; Murakoshi, K. *Appl. Phys. Lett.* **2005**, *87*, 043104.

(29) Kiguchi, M.; Konishi, T.; Miura, S.; Murakoshi, K. *Nanotechnology* **2007**, *18*, 424011.

(30) Kim, T.; Vázquez, H.; Hybertsen, M. S.; Venkataraman, L. *Nano Lett.* **2013**, *13*, 3358–64.

(31) Holze, R. In *Eectrochemical Thermodynamics and Kinetics*; Lechner, M., Ed.; Landolt-Börnstein - Group IV Physical Chemistry; Springer: Berlin, 2007; Vol. 9A; pp 223–272.

(32) Enkovaara, J.; Rostgaard, C.; Mortensen, J. J.; Chen, J.; Duak, M.; Ferrighi, L.; Gavnholt, J.; Glinsvad, C.; Haikola, V.; Hansen, H. A.; Kristoffersen, H. H.; Kuisma, M.; Larsen, A. H.; Lehtovaara, L.; Ljungberg, M.; Lopez-Acevedo, O.; Moses, P. G.; Ojanen, J.; Olsen, T.; Petzold, V.; Romero, N. A.; Stausholm-Mø ller, J.; Strange, M.; Tritsaris, G. A.; Vanin, M.; Walter, M.; Hammer, B.; Häkkinen, H.; Madsen, G. K. H.; Nieminen, R. M.; Nø rskov, J. K.; Puska, M.; Rantala, T. T.; Schiø tz, J.; Thygesen, K. S.; Jacobsen, K. W. *J. Phys.: Condens. Matter* **2010**, *22*, 253202.

(33) Meir, Y.; Wingreen, N. *Phys. Rev. Lett.* **1992**, *68*, 2512–2515.

(34) Strange, M.; Rostgaard, C.; Häkkinen, H.; Thygesen, K. S. *Phys. Rev. B: Condens. Matter Mater. Phys.* **2011**, *83*, 115108.